

GPS-denied Pedestrian Tracking in Indoor Environments Using an IMU and Magnetic Compass

W. Todd Faulkner, Robert Alwood, David W. A. Taylor, Jane Bohlin
Advanced Projects and Applications Division
ENSCO, Inc.

BIOGRAPHY

Todd Faulkner is a staff scientist with ENSCO, Inc. and has 12 years experience in geophysical signal processing and development of geolocation technologies. His areas of interest include optimal estimation, signal processing and novel applications of inertial navigation technologies. Mr. Faulkner obtained his B.S. in Geophysical Engineering from Colorado School of Mines in 1998. Faulkner.todd@ensco.com

Robert Alwood is a senior engineer with ENSCO, Inc. His technical interests include autonomous vehicles and GPS denied geolocation using inertial, RF, and optical sensors. Mr. Alwood received a B.S. in Electrical Engineering from Virginia Polytechnic Institute and State University in 2005 and is currently pursuing a M.S. in Electrical Engineering at Case Western Reserve University. alwood.robert@ensco.com

Dr. David W.A. Taylor is ENSCO's Director of Technology Development, where he leads the company's R&D programs developing sensors and systems for national security applications. He is an expert in GPS-denied navigation technologies. Dr. Taylor holds three U.S. patents with several more pending. Dr. Taylor holds the B.S. in Physics from Rhodes College and the Ph.D. in Geophysics from Virginia Tech. taylor.david@ensco.com

Jane Bohlin is a senior program manager at ENSCO, Inc. with over 15 years experience managing programs in the areas of sensor systems development, digital signal processing, data correlation and fusion, and geographic information systems (GIS). Ms. Bohlin currently manages a team of scientists and engineers working on a variety of GPS-denied navigation programs for both Government and Commercial applications. Ms. Bohlin's formal education is in software engineering. bohlin.jane@ensco.com

ABSTRACT

This paper presents an approach for pedestrian tracking based solely on the integration of a boot-mounted industrial grade inertial measurement unit (IMU) and co-located digital magnetic compass (DMC). The system is self-contained, small and requires only passive sensors (no infrastructure to set up) mounted to the heel of the operator's boot. During each footstep, there is a rest period that is detected and used to perform a zero-velocity update (ZUPT) to significantly constrain the position, velocity, roll and pitch errors through the use of an extended Kalman filter (EKF), leaving heading errors as the dominant source of position error. Heading errors accumulate with time due to integrated gyro errors and lead to computing motion in the wrong direction and hence, horizontal position errors. This paper shows that improved positioning accuracy can be achieved through the use of magnetic heading updates and a compass filter to successfully extract compass data whose measurements of the Earth's magnetic field have not been significantly distorted by the ferrous infrastructure in a typical indoor office environment.

Use of the magnetic compass filter is shown to reduce 95% horizontal position accuracies by several meters for multiple operators walking for periods of up to 15 minutes.

INTRODUCTION

Tracking and locating pedestrians in an indoor, urban or underground environment is challenging. Many users, such as first responders, war fighters and miners, operate in GPS-denied environments and work without *a priori* knowledge of their surroundings and without the benefit of pre-installed infrastructure.

Typically, a magnetic compass is disregarded as a useful component of a sensor system in these environments because of the ferrous infrastructure that distorts the measurements of the Earth's magnetic field (e.g., rebar,

wire mesh, steel framing, steel doorways, steel furniture, ferrous geology and steel shanks in the operator’s boot).

ENSCO has conducted over three years of testing in a wide range of indoor environments, ranging from wood-framed buildings while wearing non-ferrous boots to large steel-framed buildings with concrete floors reinforced with rebar while wearing boots with steel shanks. The total magnetic field strength for a range of test environments is shown in Figure 1. There is a red line in all four plots that represents the field strength recorded in a non-magnetic outdoor environment, where there was a maximum variation of a few hundredths of a Gauss. From top to bottom, in order of increasing field strength variation, the blue lines represent a walk along a sidewalk outdoors while passing parked vehicles, a demonstration walk through labs with lots of ferrous infrastructure (stairs, filing cabinets, etc..) in a concrete building at Worcester Polytechnic Institute (WPI) in Worcester, MA, a walk through multiple floors of ENSCO’s office space which is constructed of steel-studded walls and concrete floors with rebar and a walk at a government building in Virginia, respectively. In these environments, field strength variations ranged from a few hundredths of a Gauss to well over 2 Gauss.

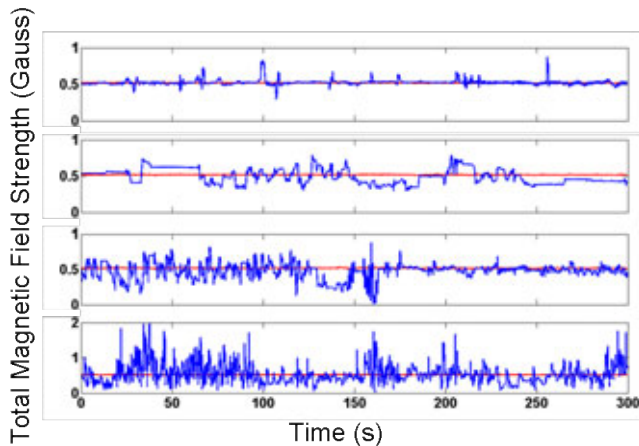


Figure 1: A range of magnetic environments have been encountered over three years of testing.

To address impacts of external environmental steel, ENSCO, Inc. has implemented a multi-stage compass filter to extract meaningful compass data in real-time to constrain inertial heading errors. Over three years of testing in multiple environments, we have found that the impact of any steel within the boot can be effectively minimized by performing a hard-magnetic calibration procedure to estimate and remove the effects generated by the steel shank [1], and that inside most steel-framed buildings, useful compass data is available at the rate of at least a few updates per minute; in wood-framed buildings, the update rate is much higher.

SYSTEM ARCHITECTURE

For boot-mounted pedestrian applications, the IMU has to be small enough to mount unobtrusively on the operator’s boot. Also, a boot-mounted IMU can experience maximum angular rates of nearly 600 °/s when walking and maximum accelerations 7-8 g’s when walking. Based on those criteria, the industrial-grade MEMSense nIMU [2], shown in Table 1, is used.

Table 1: MEMSense specifications for nIMU.

Parameter	Value
Sensor Sample Rate	150 Hz
Accelerometer Dynamic Range	+/- 10g
Accelerometer Bias (max)	0.3 m/s ²
Gyro Dynamic Range	+/- 600 deg/s
Gyro Bias (max)	1 deg/s
Gyro Bias Instability (Allan Variance characterization)	< 70 deg/hr
Compass Noise	.0056 Gauss



The core processing includes an extended Kalman filter (EKF) to integrate zero-velocity and heading observations with the position, velocity and attitude based on the integrated inertial navigation equations for each IMU measurement. The EKF state vector consists of the following 15 states:

- δr is a 3-element vector of north, east, down position errors
- δv is a 3-element vector of north, east, down velocity errors
- $\delta \psi$ is a 3-element vector of angles describing the misalignment of the body frame relative to the geographic frame
- δb^{acc} is a 3-element vector of time-correlated accelerometer errors
- δb^{gyro} is a 3-element vector of gyro time-correlated gyro errors

The dynamics equations governing the navigation system errors are based on the Ψ -angle error model [3].

Prior to navigation, the solution is initialized with a coarse alignment and initial estimate of gyro and accelerometer biases. After the initial alignment, four steps occur for each time interval an IMU measurement packet is received:

- Automatic ZUPT detection for IMU data;
- Compass filter for magnetometer data
- Integration of the differential equations governing inertial navigation [3]
- Error state covariance propagation
- EKF updates for compass and ZUPTs

A simplified block diagram describing this recursive processing architecture is shown in Figure 2.

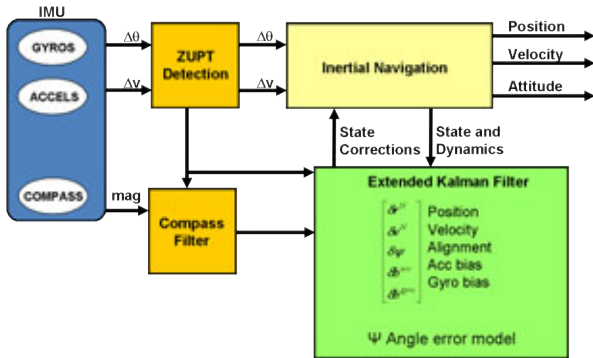


Figure 2: Core Processing Architecture.

In order to properly propagate the covariance matrix that defines error estimates for the state vector, the random IMU errors were characterized based on an Allan variance analysis of IMU data collected with the unit stationary [4].

Simple integration of the inertial navigation equations quickly leads to the accumulation of position errors as shown in Figure 3. Without the integration of external aiding measurements that relate to the position, velocity or attitude, even a navigation grade IMU results in position errors that exceed a meter after 3 minutes.

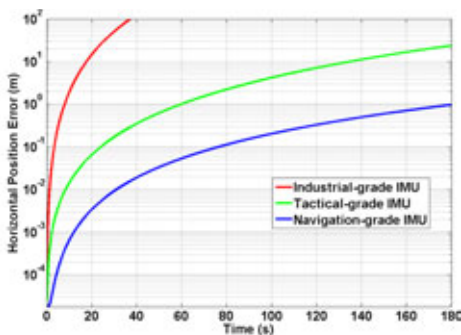


Figure 3: Inertial navigation position errors (shown for three grades of IMU sensors based solely on random IMU errors) are sufficiently large after only three minutes that an integration of external measurements is necessary to pedestrian tracking requirements.

For this application, the primary aiding measurement is a ZUPT. The IMU is mounted on the boot of the operator as shown in Figure 4 to take advantage of a stationary period between each footstep. This stationary period is detected algorithmically from the raw accelerometer and gyro data (accelerometer data shown in Figure 5) and is used to provide a ZUPT to the Kalman filter. This ZUPT constrains position, velocity and misalignment errors relative to gravity each time the foot comes to rest. Simulation using the random noise characterization of the nIMU shows that horizontal position errors are reduced

by an order of magnitude over a 10 second period when using ZUPTs as aids compared to unaided inertial navigation as shown in Figure 6. When using a high-quality IMU with gyros sensitive enough to measure the Earth's rotation, a ZUPT also provides a heading error correction. However, no heading error correction is available using a low quality IMU, so heading errors will grow if only using ZUPTs as aids.



Figure 4: MEMSense nIMU mounted on operator's boot.

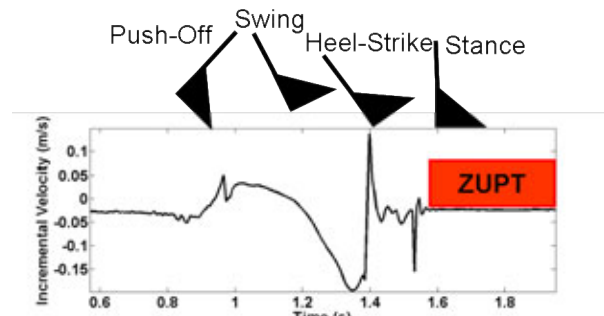


Figure 5: Raw accelerometer data showing portion of footstep where foot is stationary (shown in red), providing the Kalman filter with a ZUPT.

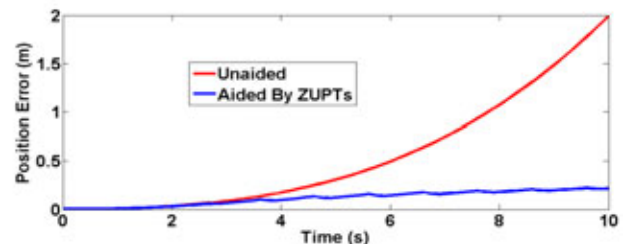


Figure 6: Horizontal position errors are reduced by an order of magnitude over 10 seconds when using a boot-mounted nIMU based solely on ZUPTs at each footstep.

Gyro bias instability is a measure of the best estimate of the gyro bias that can be computed without an external measurement. Inertial navigation heading errors are small relative to magnetic heading errors over short periods of time but increase roughly linearly over long periods of time due to gyro bias instability. Magnetic heading errors, on the other hand, are large relative to inertial navigation heading errors over short periods of time but are stable over long periods of time. In a non-magnetic environment, magnetic heading errors from a series of compass measurements are essentially uncorrelated and

are well suited to constrain the increase in inertial navigation heading errors. In a realistic indoor scenario, magnetic heading errors from a series of compass measurements are correlated as the operator passes ferrous infrastructure.

MULTI-STAGE COMPASS FILTER

A multi-stage compass filter algorithm is used to reject the majority of the compass data that are corrupted by magnetic disturbances. If any of the conditions in a stage are not met, then a heading update is not performed based on the current DMC data.

Stage 1: The first stage utilizes the difference in total magnetic field strength magnitude between the computed Earth's magnetic field strength (International Geomagnetic Reference Field model used) and the DMC measured field strength to reject data that exceeds an empirically defined threshold.

Stage 2a: This stage of the filter consists of computing the difference between the change in the magnetic heading $\Delta\varphi_-^{DMC}$ computed from the DMC measurements and the change in the navigation heading, $\Delta\varphi_-^{nav}$ computed from the Kalman filtered IMU data over a user-defined period of time $t_{current} - t_{previous}$. DMC data are rejected if $|\Delta\varphi_{current-previous}^{nav-DMC}|$ exceeds an empirically defined threshold.

$$\Delta\varphi_-^{nav} = \varphi_{current}^{nav} - \varphi_{previous}^{nav} \quad (1.1)$$

$$\Delta\varphi_-^{DMC} = \varphi_{current}^{DMC} - \varphi_{previous}^{DMC} \quad (1.2)$$

$$\Delta\varphi_{current-previous}^{nav-DMC} = \Delta\varphi_-^{nav} - \Delta\varphi_-^{DMC} \quad (1.3)$$

Stage 2b: If the conditions of stage 2a are not satisfied, then the next step consists of integrating the inertial navigation equations describing attitude over a user-defined period of time, $t_{next} - t_{current}$, and then computing the difference between the change in the magnetic heading, $\Delta\varphi_+^{DMC}$, and the change in the navigation heading, $\Delta\varphi_+^{nav}$, over that same period of time and rejecting the DMC data if $|\Delta\varphi_{next-current}^{nav-DMC}|$ exceeds an empirically defined threshold.

$$\Delta\varphi_+^{nav} = \varphi_{next}^{nav} - \varphi_{current}^{nav} \quad (1.4)$$

$$\Delta\varphi_+^{DMC} = \varphi_{next}^{DMC} - \varphi_{current}^{DMC} \quad (1.5)$$

$$\Delta\varphi_{next-current}^{nav-DMC} = \Delta\varphi_+^{nav} - \Delta\varphi_+^{DMC} \quad (1.6)$$

Stage 2b requires the filter to operate with a fixed-lag time and can be omitted for real-time applications or implemented as a near-real-time process.

COMPASS FILTER RESULTS

Extensive tests have been conducted at ENSCO's office building in Springfield, VA, which consists of steel-studded walls, concrete floors reinforced with rebar and several stairwells. The ability of the compass filter to reject distorted magnetic field measurements is shown in Figure 7 through Figure 9 for an operator performing a 15-minute walk through this building. For all of the plots, magnetic heading has been compensated for local magnetic declination.

The relative altitude change for operator #1 is shown in red in the top plot of Figure 7, and the corresponding magnetic field strength recorded along the walk is shown in the lower plot. Additionally, the black asterisks indicate that the conditions of both stages of the compass filter have been met.

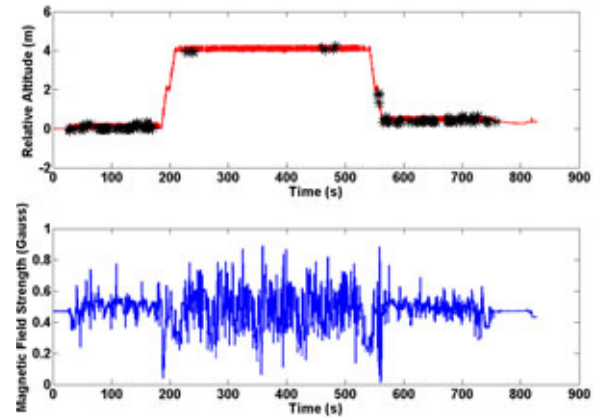


Figure 7: The top plot shows the relative altitude estimate in red and black asterisks that signify that the conditions of both stages of the compass filter were met. The bottom plot shows the total magnetic field strength (blue).

As can be seen in Figure 7, the variation in magnetic field strength was much larger on the second floor of the building and only a few compass measurements per minute successfully met the conditions of both stages of the compass filter. On the first floor, approximately 20 compass measurements per minute successfully met the conditions. Figure 8 shows one minute of the operator's path (from 660 to 720 seconds in Figure 7) along the first floor when compass updates are numerous. Figure 9 shows one minute of the operator's path (from 420 to 480 seconds in Figure 7) along the second floor when there are only two compass updates and differences between magnetic and inertial navigation heading are generally large (up to almost 90 degrees).

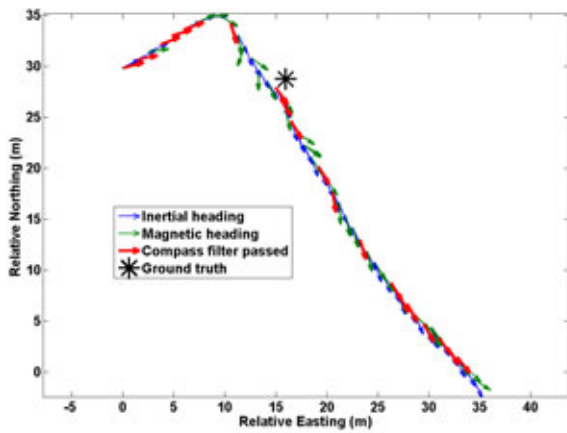


Figure 8: When walking on the first floor of the building (660s to 720s in Figure 7), compass updates were plentiful. In this quiver plot, a unit vector is plotted at each footstep to indicate the inertial heading in blue, rejected magnetic headings in green and used magnetic headings in red. The black asterisks are ground truth markers.

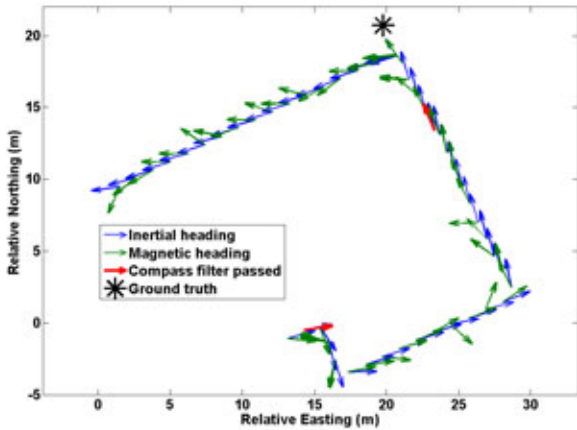


Figure 9: When walking on the second floor of the building (420s to 480s in Figure 7), there were only two compass updates during the minute of data shown. In this quiver plot, a unit vector is plotted at each footstep to indicate the inertial heading in blue, rejected magnetic headings in green and used magnetic headings in red. The black asterisks are ground truth markers.

Figure 10 shows an outdoor environment with the operator walking down the sidewalk past a parked truck. The compass filter successfully rejects the compass measurements that are distorted when walking past the truck, but successfully locates other useful magnetic data in spite of the reinforced concrete sidewalk.

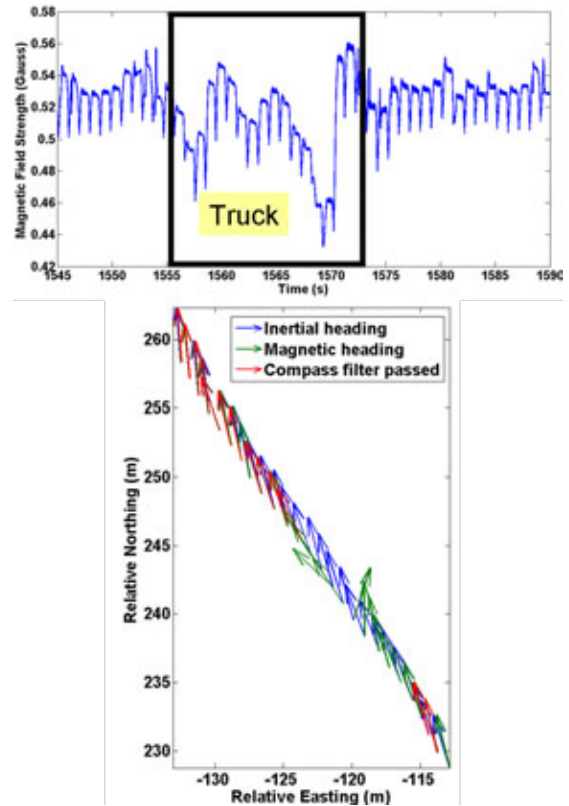


Figure 10: Top plot shows total magnetic field strength recorded when walking along a sidewalk past a truck parked alongside the road. In quiver plot below it, a unit vector is plotted at each footstep to indicate the inertial heading in blue, rejected magnetic headings in green and used magnetic headings in red.

The random error in the magnetic vector components measured by the compass (one standard deviation equals .0056 Gauss) is large enough to generate over a degree of heading error. For outdoor magnetic environments, there may be some benefit to using a lower noise compass. However, for inside environments, the correlated magnetic measurement errors due to infrastructure are large relative to the random error, so a better compass (lower random error) will not significantly impact the output of the compass filter and hence, will not improve position accuracy.

HEADING ERROR OBSERVABILITY

When considering whether a compass can be useful to constrain heading errors from an IMU in a magnetically noisy environment, it must be shown that there is an observable difference between the heading based solely on an IMU and the magnetic heading (corrected for local declination). The bottom plot in Figure 7 shows the total magnetic field strength as recorded by the compass during a 14-minute walk covering 850 meters through an ENSCO office building in Springfield, VA. Figure 11 shows a corresponding difference in heading between the

IMU (red) and compass (blue) that was computed during the walk.

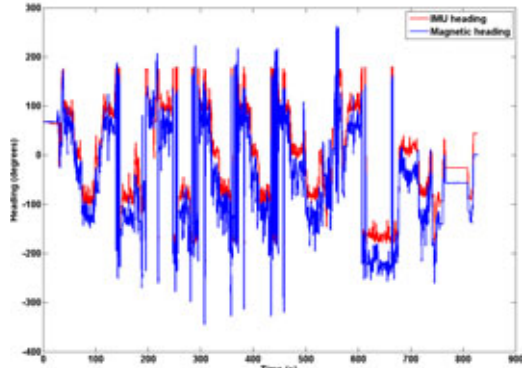


Figure 11: A difference is seen in heading solely based on an IMU (in red) and magnetic heading that has been corrected for local declination (in blue).

There is an average heading difference of about 34° during the first 3 minutes of the walk and an average heading difference of about 46° during the last 4 minutes. The initial heading difference of 34° is simply the initial orientation correction, with the remaining 12° heading drift accumulating over the 14-minute walk. This drift of 12° in 14 minutes is consistent with the gyro bias instability of $\sim 70^\circ/\text{hr}$ for the nIMU.

In Figure 12, ground truth markers that were crossed during the data collection are indicated by the black asterisks. The estimated path and marker locations without the use of the compass are shown by the blue line and blue asterisks, respectively. The estimated path and marker locations with the use of the compass and compass filter are shown by the red line and red asterisks, respectively. The use of heading updates when the conditions of both stages of the compass filter are met greatly improves the position accuracy, reducing the errors for these two points to a few meters after about 12 minutes of walking.

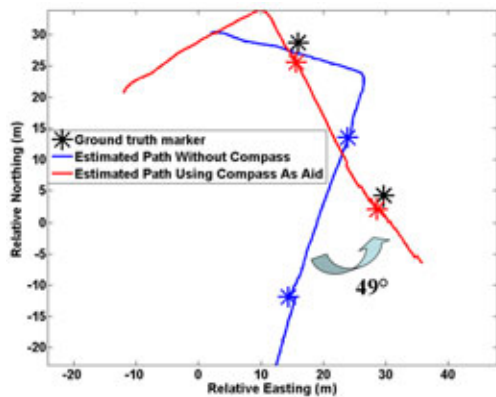


Figure 12: Estimated paths are shown with and without the use of the compass in red and blue, respectively. This segment of data corresponds in time to the end of the walk and shows a corresponding

difference in ground track heading of 49° (close to the 46° mean difference in heading).

POSITIONING RESULTS USING COMPASS FILTER

ENSCO conducted an acceptance test in conjunction with Rex Systems, Inc. under contract W15P7T-05-C-P225 to the US Army's Communications, Electronics Research, Development, and Engineering Center (CERDEC) in February 2008. The goal was to track four operators walking an indoor path for 15 minutes with a 95% horizontal position accuracy of 3 meters (95% of all estimated positions lie within 3 meters of the known positions in the horizontal plane).

Since the test was for a first responder application, the IMU was mounted on the heel of a firefighter boot as shown in Figure 13, and a hard magnetic compass calibration procedure was performed to account for the steel shank in the boots.



Figure 13: IMU mounted on heel of firefighter's boot.

The test was conducted at ENSCO, Inc. in a typical two-story commercial office building along the path shown in Figure 14.

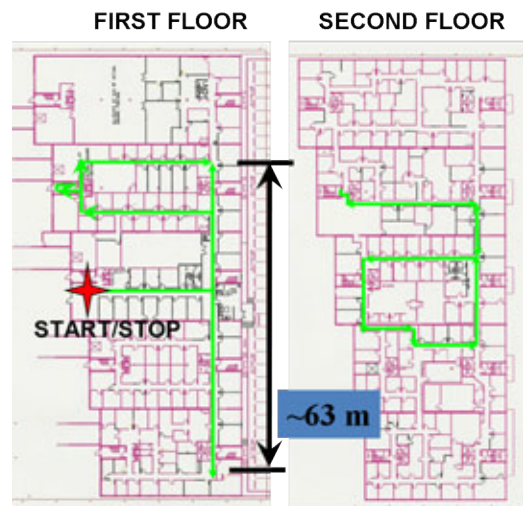


Figure 14: The green lines show the footprint of the path that the operators walked for 15 minutes which

includes multiple loops, multiple floors via a flight of stairs and the same start and stop location (red star).

Each operator passed over a series of professionally surveyed ground truth locations that were passed 27 times during the collection to allow for quantitative position error analysis.

For comparison, data were processed using the correct initial heading and then both with and without the use of the compass filtered data. A summary of the horizontal position errors for the four operators based on the 27 ground truth locations is shown in Table 2. For both operators, the 95% horizontal accuracy improved when both stages of the compass filter were used.

Table 2: Horizontal position errors are shown for 15-minute indoor walking acceptance test with and without the use of a compass.

	95% Horizontal Accuracy (m)	
	Not Using Compass	Using Compass
Operator #1	7.9	2.8
Operator #2	17.2	4.0
Operator #3	11.9	6.8
Operator #4	9.8	7.1

CONCLUSIONS

Improved positioning accuracy can be achieved through the integration of filtered compass data in an indoor environment. For low-quality IMUs, even sparse updates on the order of a few per minute can significantly reduce heading errors and improve position accuracy. A compass filter is shown that can successfully extract these useful compass measurements and reject distorted magnetic measurements efficiently and in real-time. In most environments, these distorted magnetic measurements due to local ferrous infrastructure are large relative to compass sensor noise floors, so a higher quality (lower noise) compass will not significantly improve the results.

REFERENCES

- [1] Gebre-Egziabher, D., G. Elkaim, J. D. Powell, B. Parkinson, "A Non-linear, Two-step Estimation Algorithm for Calibrating Solid-state Strapdown Magnetometers", 8th International St. Petersburg Conference on Navigation Systems (IEEE/AIAA), St. Petersburg, Russia, May 27-May 31, 2001.
- [2] MEMSense, *nIMU Nano Inertial Measurement Unit Series Documentation*, Version 2.9, 2007.

- [3] Rogers, R. M., *Applied Mathematics in Integrated Navigation Systems*, AIAA, 2000.
- [4] Hou, Haiying and El-Sheimy, N., "Inertial Sensors Errors Modeling Using Allan Variance", ION GNSS, 2003.